

Vector Field Topology of Time-Dependent Flows in a Steady Reference Frame – Additional Material

Irene Baeza Rojo and Tobias Günther



1 INTRODUCTION

This document contains the derivations for the main paper. Section 2 describes the forward and backward displacement transformation. Section 3 shows how existing reference frame transformations appear as special cases. In Section 4, the derivatives of the transformed vector field are calculated. Section 5 describes the general construction of our system matrix in Taylor approximation. The system matrix construction of other basis representations and their results are described in Section 6. The analytic vector fields of the main paper are described in detail in Section 7. Section 8 shows further experiments and results of our reference frame optimization and topology extraction.

2 DISPLACEMENT TRANSFORMATIONS

In the following, we derive the spatially-varying forward and backward transformation of a vector field.

2.1 Forward Transformation

Given is a space-time displacement vector field $\mathbf{F}(\mathbf{x}, t)$ that moves a point \mathbf{x} to its new location \mathbf{x}^* :

$$\mathbf{x}^* = \mathbf{x} + \mathbf{F}(\mathbf{x}, t). \quad (1)$$

By considering a pathline $\mathbf{x}(t)$ in Eq. (1) and by computing its temporal derivative, we can observe how the tangent of the pathline $\mathbf{x}(t)$ behaves under the general displacement transformation.

$$\frac{d\mathbf{x}^*(t)}{dt} = \frac{d\mathbf{x}(t)}{dt} + \frac{D\mathbf{F}(\mathbf{x}(t), t)}{Dt} \quad (2)$$

$$= \frac{d\mathbf{x}(t)}{dt} + \nabla\mathbf{F}(\mathbf{x}(t), t) \cdot \frac{d\mathbf{x}(t)}{dt} + \mathbf{F}_t(\mathbf{x}(t), t) \quad (3)$$

$$= [\mathbf{I} + \nabla\mathbf{F}(\mathbf{x}(t), t)] \cdot \frac{d\mathbf{x}(t)}{dt} + \mathbf{F}_t(\mathbf{x}(t), t) \quad (4)$$

Since pathlines are tangential to a vector field $\mathbf{v}(\mathbf{x}(t), t) = \frac{d\mathbf{x}(t)}{dt}$, Eq. (4) can be rephrased by substitution, which yields:

$$\mathbf{v}^*(\mathbf{x}^*, t) = [\mathbf{I} + \nabla\mathbf{F}(\mathbf{x}, t)] \cdot \mathbf{v}(\mathbf{x}, t) + \mathbf{F}_t(\mathbf{x}, t). \quad (5)$$

2.2 Backward Transformation

By rearranging Eq. (1) the backward transformation becomes:

$$\mathbf{x} = \mathbf{x}^* - \mathbf{F}(\mathbf{x}, t). \quad (6)$$

Again, by considering the tangent of a pathline $\mathbf{x}(t)$:

$$\frac{d\mathbf{x}(t)}{dt} = \frac{d\mathbf{x}^*(t)}{dt} - \frac{D\mathbf{F}(\mathbf{x}(t), t)}{Dt} \quad (7)$$

$$= \frac{d\mathbf{x}^*(t)}{dt} - \nabla\mathbf{F}(\mathbf{x}(t), t) \cdot \frac{d\mathbf{x}(t)}{dt} - \mathbf{F}_t(\mathbf{x}(t), t) \quad (8)$$

$$= [\mathbf{I} + \nabla\mathbf{F}(\mathbf{x}(t), t)]^{-1} \frac{d\mathbf{x}^*(t)}{dt} - \mathbf{F}_t(\mathbf{x}(t), t) \quad (9)$$

we arrive at the expression for the transformation of a vector field:

$$\mathbf{v}(\mathbf{x}, t) = [\mathbf{I} + \nabla\mathbf{F}(\mathbf{x}, t)]^{-1} (\mathbf{v}^*(\mathbf{x} + \mathbf{F}(\mathbf{x}, t), t) - \mathbf{F}_t(\mathbf{x}, t)) \quad (10)$$

2.3 Change of Variables

The conversion between the two spaces requires us to consider the coordinate Jacobians in order to change variables:

$$\frac{\partial\mathbf{x}^*}{\partial\mathbf{x}} = \mathbf{I} + \nabla\mathbf{F}(\mathbf{x}, t) \quad \frac{\partial\mathbf{x}}{\partial\mathbf{x}^*} = [\mathbf{I} + \nabla\mathbf{F}(\mathbf{x}, t)]^{-1} \quad (11)$$

The two expressions follow by differentiation from Eqs. (1) and (6) and are used to study how coordinate changes in the input space relate to coordinate changes in the transformed space.

3 SPECIAL CASES OF TRANSFORMATIONS

Next, we cover special cases of Eqs. (1), (5), (6) and (10), i.e., equal-speed translations (Galilean transformations) and temporally-varying rotations and translations (objective transformations), and temporally-varying affine transformations. Note that all these transformations have in common that $\nabla(\nabla\mathbf{F}(\mathbf{x}, t)) = \mathbf{0}$, i.e., they are homogeneous deformations.

3.1 Galilean Transformation

For a Galilean transformation we have a spatially-constant transformation $\mathbf{F}(\mathbf{x}, t) = t \cdot \mathbf{c}_1 + \mathbf{c}_0$. Since $\nabla\mathbf{F}(\mathbf{x}, t) = \mathbf{0}$ and $\frac{\partial\mathbf{F}(\mathbf{x}, t)}{\partial t} = \mathbf{F}_t(\mathbf{x}, t) = \mathbf{c}_1$, a forward transformation has the form:

$$\mathbf{x}^* = \mathbf{x} + t \cdot \mathbf{c}_1 + \mathbf{c}_0 \quad (12)$$

$$\mathbf{v}^*(\mathbf{x}^*, t) = \mathbf{v}(\mathbf{x}, t) + \mathbf{c}_1 \quad (13)$$

where \mathbf{c}_0 and \mathbf{c}_1 are constant vectors. The backward transformation therefore becomes:

$$\mathbf{x} = \mathbf{x}^* - t \cdot \mathbf{c}_1 - \mathbf{c}_0 \quad (14)$$

$$\mathbf{v}(\mathbf{x}, t) = \mathbf{v}^*(\mathbf{x}^*, t) - \mathbf{c}_1 \quad (15)$$

3.2 Objective Transformation

For an objective transformation, we have $\mathbf{F}(\mathbf{x}, t) = [\mathbf{R}(t) - \mathbf{I}]\mathbf{x} + \mathbf{c}(t)$, where $\mathbf{R}(t)$ is a rotation matrix and $\mathbf{c}(t)$ is a translation vector. Since both are spatially constant, we have $\nabla\mathbf{F}(\mathbf{x}, t) = \mathbf{R}(t) - \mathbf{I}$ and the time partial is $\frac{\partial\mathbf{F}(\mathbf{x}, t)}{\partial t} = \mathbf{F}_t(\mathbf{x}, t) = \mathbf{R}_t(t) \cdot \mathbf{x} + \mathbf{c}_t(t)$. We get:

$$\mathbf{x}^* = \mathbf{R}(t) \cdot \mathbf{x} + \mathbf{c}(t) \quad (16)$$

$$\mathbf{v}^*(\mathbf{x}^*, t) = \mathbf{R}(t) \cdot \mathbf{v}(\mathbf{x}, t) + \mathbf{R}_t(t) \cdot \mathbf{x} + \mathbf{c}_t(t) \quad (17)$$

Then, the inverse transformation becomes after simplification:

$$\mathbf{x} = \mathbf{R}(t)^T (\mathbf{x}^* - \mathbf{c}(t)) \quad (18)$$

$$\mathbf{v}(\mathbf{x}, t) = \mathbf{R}(t)^T [\mathbf{v}^*(\mathbf{x}^*, t) - \mathbf{c}_t(t)] + \mathbf{R}_t(t)^T [\mathbf{x}^* - \mathbf{c}(t)] \quad (19)$$

3.3 Affine Transformation

For an affine transformation, we have $\mathbf{F}(\mathbf{x}, t) = [\mathbf{Q}(t) - \mathbf{I}]\mathbf{x} + \mathbf{c}(t)$, where $\mathbf{Q}(t)$ is a general matrix and $\mathbf{c}(t)$ is a translation vector. Since both are spatially constant, we have $\nabla\mathbf{F}(\mathbf{x}, t) = \mathbf{Q}(t) - \mathbf{I}$ and the time partial is $\frac{\partial\mathbf{F}(\mathbf{x}, t)}{\partial t} = \mathbf{F}_t(\mathbf{x}, t) = \mathbf{Q}_t(t) \cdot \mathbf{x} + \mathbf{c}_t(t)$. We get:

$$\mathbf{x}^* = \mathbf{Q}(t) \cdot \mathbf{x} + \mathbf{c}(t) \quad (20)$$

$$\mathbf{v}^*(\mathbf{x}^*, t) = \mathbf{Q}(t) \cdot \mathbf{v}(\mathbf{x}, t) + \mathbf{Q}_t(t) \cdot \mathbf{x} + \mathbf{c}_t(t) \quad (21)$$

• Irene Baeza Rojo and Tobias Günther are with the Computer Graphics Laboratory, ETH Zürich. E-mail: irene.baeza|tobias.guenther@inf.ethz.ch.

Then, the inverse transformation becomes after simplification:

$$\mathbf{x} = \mathbf{Q}(t)^{-1}(\mathbf{x}^* - \mathbf{c}(t)) \quad (22)$$

$$\mathbf{v}(\mathbf{x}, t) = \mathbf{Q}(t)^{-1}[\mathbf{v}^*(\mathbf{x}^*, t) - \dot{\mathbf{c}}(t)] + \mathbf{Q}_t(t)^{-1}[\mathbf{x}^* - \mathbf{c}(t)] \quad (23)$$

In the context of continuum mechanics, the affine transformation is what is usually referred to as the general homogeneous deformation.

4 DERIVATION OF DERIVATIVES

In order to compute the time partial in the new reference frame after forward transformation, we first compute the acceleration \mathbf{a}^* and the Jacobian $\nabla \mathbf{v}^*$. By expressing the velocity in Eq. (5) with total derivatives instead of partial derivatives, we obtain:

$$\mathbf{v}^*(\mathbf{x}^*, t) = \mathbf{v}(\mathbf{x}, t) + \frac{D\mathbf{F}(\mathbf{x}, t)}{Dt} \quad (24)$$

In the following, several total derivatives are needed:

$$\frac{D\mathbf{F}(\mathbf{x}, t)}{Dt} = \nabla \mathbf{F}(\mathbf{x}, t) \cdot \mathbf{v}(\mathbf{x}, t) + \mathbf{F}_t(\mathbf{x}, t) \quad (25)$$

$$\frac{D\nabla \mathbf{F}(\mathbf{x}, t)}{Dt} = \nabla(\nabla \mathbf{F}(\mathbf{x}, t)) \cdot \mathbf{v}(\mathbf{x}, t) + \nabla \mathbf{F}_t(\mathbf{x}, t) \quad (26)$$

$$\frac{D\mathbf{F}_t(\mathbf{x}, t)}{Dt} = \nabla \mathbf{F}_t(\mathbf{x}, t) \cdot \mathbf{v}(\mathbf{x}, t) + \mathbf{F}_{tt}(\mathbf{x}, t) \quad (27)$$

$$\nabla \frac{D\mathbf{F}(\mathbf{x}, t)}{Dt} = \frac{D\nabla \mathbf{F}(\mathbf{x}, t)}{Dt} + \nabla \mathbf{F}(\mathbf{x}, t) \cdot \mathbf{J}(\mathbf{x}, t) \quad (28)$$

Since we consider the total derivatives along pathlines $\mathbf{v}(\mathbf{x}, t) = \frac{d\mathbf{x}}{dt}$, these are also called material derivatives.

The total time derivative of \mathbf{v}^* gives the acceleration \mathbf{a}^* :

$$\mathbf{a}^*(\mathbf{x}^*, t) = \frac{D\mathbf{v}^*(\mathbf{x}^*, t)}{Dt} = \mathbf{a}(\mathbf{x}, t) + \frac{D^2\mathbf{F}(\mathbf{x}, t)}{Dt^2} \quad (29)$$

$$\begin{aligned} &= \mathbf{a}(\mathbf{x}, t) + \frac{D\nabla \mathbf{F}(\mathbf{x}, t)}{Dt} \cdot \mathbf{v}(\mathbf{x}, t) + \nabla \mathbf{F}(\mathbf{x}, t) \cdot \mathbf{a}(\mathbf{x}, t) + \frac{D\mathbf{F}_t(\mathbf{x}, t)}{Dt} \\ &= [\mathbf{I} + \nabla \mathbf{F}(\mathbf{x}, t)] \cdot \mathbf{a}(\mathbf{x}, t) + \frac{D\nabla \mathbf{F}(\mathbf{x}, t)}{Dt} \cdot \mathbf{v}(\mathbf{x}, t) + \frac{D\mathbf{F}_t(\mathbf{x}, t)}{Dt} \end{aligned}$$

The Jacobian is computed from partial differentiation with respect to space. Note that a change of variables is applied, using Eq. (11).

$$\mathbf{J}^*(\mathbf{x}^*, t) = \frac{\partial \mathbf{v}^*(\mathbf{x}^*, t)}{\partial \mathbf{x}^*} = \frac{\partial \mathbf{v}(\mathbf{x}, t)}{\partial \mathbf{x}} \frac{\partial \mathbf{x}}{\partial \mathbf{x}^*} + \frac{\partial D\mathbf{F}(\mathbf{x}, t)}{\partial \mathbf{x} Dt} \frac{\partial \mathbf{x}}{\partial \mathbf{x}^*} \quad (30)$$

$$= \left[\mathbf{J}(\mathbf{x}, t) + \nabla \frac{D\mathbf{F}(\mathbf{x}, t)}{Dt} \right] \cdot [\mathbf{I} + \nabla \mathbf{F}(\mathbf{x}, t)]^{-1} \quad (31)$$

Finally, the velocity time partial \mathbf{v}_t^* is computed using

$$\mathbf{v}_t^*(\mathbf{x}^*, t) = \mathbf{a}^*(\mathbf{x}^*, t) - \mathbf{J}^*(\mathbf{x}^*, t) \cdot \mathbf{v}^*(\mathbf{x}^*, t) \quad (32)$$

$$\begin{aligned} &= \mathbf{v}_t(\mathbf{x}, t) + \nabla \mathbf{F}(\mathbf{x}, t) \cdot \mathbf{v}_t(\mathbf{x}, t) + \frac{D\mathbf{F}_t(\mathbf{x}, t)}{Dt} \\ &\quad - \left[\mathbf{J}(\mathbf{x}, t) + \nabla \frac{D\mathbf{F}(\mathbf{x}, t)}{Dt} \right] \cdot [\mathbf{I} + \nabla \mathbf{F}(\mathbf{x}, t)]^{-1} \cdot \mathbf{F}_t(\mathbf{x}, t) \end{aligned} \quad (33)$$

5 CONSTRUCTION OF SYSTEM MATRIX

In order to adapt to spatial variations of \mathbf{F}_t and \mathbf{G} within the neighborhood U , we spatially discretized the derivatives by a component-wise multi-variate m -th order Taylor expansion around the observation point \mathbf{x}_0 , i.e., the center of neighborhood region U :

$$\mathbf{F}_t(\mathbf{x}, t) = \sum_{m=0}^{\infty} \frac{1}{m!} \nabla^m \mathbf{F}_t(\mathbf{x}_0, t) \cdot (\mathbf{x} - \mathbf{x}_0)^m \quad (34)$$

$$\nabla \mathbf{F}_t(\mathbf{x}, t) = \sum_{m=1}^{\infty} \frac{1}{(m-1)!} \nabla^m \mathbf{F}_t(\mathbf{x}_0, t) \cdot (\mathbf{x} - \mathbf{x}_0)^{m-1} \quad (35)$$

$$\mathbf{G}(\mathbf{x}, t) = \sum_{m=0}^{\infty} \frac{1}{m!} \nabla^m \mathbf{G}(\mathbf{x}_0, t) \cdot (\mathbf{x} - \mathbf{x}_0)^m \quad (36)$$

with $\nabla^m \mathbf{F}_t(\mathbf{x}_0, t)$ and $\nabla^m \mathbf{G}(\mathbf{x}_0, t)$ being symmetric tensors of order m .

To simplify the notation we set $\mathbf{F}_t^{(m)} = \nabla^m \mathbf{F}_t(\mathbf{x}_0, t)$ and $\mathbf{G}^{(m)} = \nabla^m \mathbf{G}(\mathbf{x}_0, t)$. By inserting Eqs. (34)–(36) into the time partial derivative, we obtained the time partial $\mathbf{v}_t^*(\mathbf{x}, t)|_{t=t_0}$ in Taylor expansion:

$$\begin{aligned} \mathbf{v}_t^*(\mathbf{x}, t)|_{t=t_0} &= \mathbf{v}_t(\mathbf{x}, t) \\ &+ \sum_{m=0}^{\infty} \left[\mathbf{F}_t^{(m)} \cdot \frac{\mathbf{x}^{m-1}}{(m-1)!} \cdot \mathbf{v}(\mathbf{x}, t) - \mathbf{J}(\mathbf{x}, t) \cdot \mathbf{F}_t^{(m)} \cdot \frac{\mathbf{x}^m}{m!} \right] \\ &+ \sum_{m=0}^{\infty} \mathbf{G}^{(m)} \cdot \frac{\mathbf{x}^m}{m!} \end{aligned} \quad (37)$$

Minimizing Eq. (37) led us to the linear system:

$$\mathbf{M}(\mathbf{x}, t) \cdot \mathbf{p}(\mathbf{x}, t) = -\mathbf{v}_t(\mathbf{x}, t) \quad (38)$$

with the system matrix \mathbf{M} containing a series of squared matrices

$$\mathbf{M} = \left(\underbrace{\mathbf{F}_{00}, \mathbf{G}_{00}}_{\text{zero-order}}, \underbrace{\mathbf{F}_{10}, \mathbf{G}_{10}, \mathbf{F}_{01}, \mathbf{G}_{01}}_{\text{first-order}}, \underbrace{\mathbf{F}_{20}, \mathbf{G}_{20}, \mathbf{F}_{11}, \mathbf{G}_{11}, \mathbf{F}_{02}, \mathbf{G}_{02}}_{\text{second-order}}, \dots \right) \quad (39)$$

In the following, we look at the construction of the matrix in Eq. (39).

5.1 Construction in 2D

The tensor products in Eqs. (34)–(36) can be expressed as:

$$\mathbf{F}_t(\mathbf{x}, t) = \sum_{m=0}^{\infty} \sum_{i=0}^m \frac{x^i y^j}{i! j!} \mathbf{f}_{i,j} \quad (40)$$

$$\nabla \mathbf{F}_t(\mathbf{x}, t) = \sum_{m=0}^{\infty} \sum_{i=0}^{m-1} \frac{x^i y^{j-1}}{i! (j-1)!} [\mathbf{f}_{i+1, j-1}, \mathbf{f}_{i, j}] \quad (41)$$

$$\mathbf{G}(\mathbf{x}, t) = \sum_{m=0}^{\infty} \sum_{i=0}^m \frac{x^i y^j}{i! j!} \mathbf{g}_{i,j} \quad (42)$$

with \mathbf{f}_{ij} and \mathbf{g}_{ij} being the vector-valued entries in the symmetric tensors for $i + j = m$. After inserting Eqs. (46)–(47) into Eq. (37), we get the following system matrix entries \mathbf{F}_{ij} and \mathbf{G}_{ij} for the corresponding unknown vector-valued coefficients \mathbf{f}_{ij} and \mathbf{g}_{ij} :

$$\mathbf{F}_{ij} = \underbrace{\frac{u x^{i-1} y^j}{(i-1)! j!}}_{i \neq 0} \mathbf{I} + \underbrace{\frac{v x^i y^{j-1}}{i! (j-1)!}}_{j \neq 0} \mathbf{I} - \frac{x^i y^j}{i! j!} \mathbf{J}, \quad \mathbf{G}_{ij} = \frac{x^i y^j}{i! j!} \mathbf{I} \quad (43)$$

If the entries \mathbf{F}_{ij} and \mathbf{G}_{ij} are sorted as shown in Eq. (39), the linear array index in \mathbf{p} for the corresponding coefficients \mathbf{F}_{ij} is $(i+j)(i+j+1)+2j$. For reference, the terms up to third order ($m=3$) are listed below:

$$\begin{aligned} &(\mathbf{F}_{00}, \mathbf{F}_{10}, \mathbf{F}_{01}, \mathbf{F}_{20}, \mathbf{F}_{11}, \mathbf{F}_{02}, \mathbf{F}_{30}, \mathbf{F}_{21}, \mathbf{F}_{12}, \mathbf{F}_{03}) = \quad (44) \\ &\underbrace{\left(-\mathbf{J} \right)}_{\text{zero-order}} \underbrace{\left(u\mathbf{I} - x\mathbf{J} \quad v\mathbf{I} - y\mathbf{J} \right)}_{\text{first-order}} \underbrace{\left(ux\mathbf{I} - \frac{x^2}{2}\mathbf{J} \quad uy\mathbf{I} + vx\mathbf{I} - xy\mathbf{J} \quad vy - \frac{y^2}{2}\mathbf{J} \right)}_{\text{second-order}} \dots \\ &\underbrace{\left(\frac{ux^2}{2}\mathbf{I} - \frac{x^3}{6}\mathbf{J} \quad uxy\mathbf{I} + \frac{vx^2}{2}\mathbf{I} - \frac{x^2y}{2}\mathbf{J} \quad \frac{uy^2}{2}\mathbf{I} + vxy\mathbf{I} - \frac{xy^2}{2}\mathbf{J} \quad \frac{vy^2}{2} - \frac{y^3}{6}\mathbf{J} \right)}_{\text{third-order}} \end{aligned}$$

$$\begin{aligned} &(\mathbf{G}_{00}, \mathbf{G}_{10}, \mathbf{G}_{01}, \mathbf{G}_{20}, \mathbf{G}_{11}, \mathbf{G}_{02}, \mathbf{G}_{30}, \mathbf{G}_{21}, \mathbf{G}_{12}, \mathbf{G}_{03}) = \quad (45) \\ &\underbrace{\left(\mathbf{I} \right)}_{\text{zero-order}} \underbrace{\left(x\mathbf{I} \quad y\mathbf{I} \right)}_{\text{first-order}} \underbrace{\left(\frac{x^2}{2}\mathbf{I} \quad xy\mathbf{I} \quad \frac{y^2}{2}\mathbf{I} \right)}_{\text{second-order}} \underbrace{\left(\frac{x^2y}{2}\mathbf{I} \quad \frac{xy^2}{2}\mathbf{I} \quad \frac{y^3}{6}\mathbf{I} \right)}_{\text{third-order}} \end{aligned}$$

Note that the first-order approximation (sum of zero-order and first-order terms) leads to the affine-invariant approach of Günther and Theisel. For higher orders than shown here, use the general description in Eq. (43).

5.2 Construction in 3D

In polynomial representation, the tensor products in Eqs. (34)–(36) can be expressed as:

$$\mathbf{F}_t(\mathbf{x}, t) = \sum_{m=0}^{\infty} \sum_{i=0}^m \sum_{j=0}^{m-i} \frac{x^i y^j z^{k-1}}{i! j! k!} \mathbf{f}_{i,j,k} \quad (46)$$

$$\nabla \mathbf{F}_t(\mathbf{x}, t) = \sum_{m=0}^{\infty} \sum_{i=0}^m \sum_{j=0}^{m-i-1} \frac{x^i y^j z^{k-1}}{i! j! (k-1)!} [\mathbf{f}_{i+1,j,k-1}, \mathbf{f}_{i,j+1,k-1}, \mathbf{f}_{i,j,k}]$$

$$\mathbf{G}(\mathbf{x}, t) = \sum_{m=0}^{\infty} \sum_{i=0}^m \sum_{j=0}^{m-i} \frac{x^i y^j z^k}{i! j! k!} \mathbf{g}_{i,j,k} \quad (47)$$

with \mathbf{f}_{ijk} and \mathbf{g}_{ijk} being vector-valued entries in the symmetric tensors for $i + j + k = m$. After inserting Eqs. (46)–(47) into Eq. (37), we get the system matrix entries \mathbf{F}_{ijk} and \mathbf{G}_{ijk} for the corresponding unknown vector-valued coefficients \mathbf{f}_{ijk} and \mathbf{g}_{ijk} :

$$\mathbf{F}_{ijk} = \underbrace{\frac{ux^{i-1}y^jz^k}{(i-1)!j!k!}}_{i \neq 0} \mathbf{I} + \underbrace{\frac{vx^iy^{j-1}z^k}{i!(j-1)!k!}}_{j \neq 0} \mathbf{I} + \underbrace{\frac{wx^iy^jz^{k-1}}{i!j!(k-1)!}}_{k \neq 0} \mathbf{I} - \frac{x^iy^jz^k}{i!j!k!} \mathbf{J}$$

$$\mathbf{G}_{ijk} = \frac{x^iy^jz^k}{i!j!k!} \mathbf{I} \quad (48)$$

We sort the entries \mathbf{F}_{ijk} and \mathbf{G}_{ijk} such that the linear array index in \mathbf{p} for the corresponding coefficients \mathbf{F}_{ijk} is $(i + j + k)(i + j + k + 1)(i + j + k + 2)/3 + (j + k)(j + k + 1) + 2k$. For reference, the terms up to second order ($m = 2$) are listed below:

$$(\mathbf{F}_{000}, \mathbf{F}_{100}, \mathbf{F}_{010}, \mathbf{F}_{001}, \mathbf{F}_{200}, \mathbf{F}_{110}, \mathbf{F}_{020}, \mathbf{F}_{101}, \mathbf{F}_{011}, \mathbf{F}_{002}) = \quad (49)$$

$$\left(\underbrace{-\mathbf{J}}_{\text{zero-order}} \quad \underbrace{u\mathbf{I} - x\mathbf{J} \quad v\mathbf{I} - y\mathbf{J} \quad w\mathbf{I} - z\mathbf{J}}_{\text{first-order}} \quad \underbrace{ux\mathbf{I} - \frac{x^2}{2}\mathbf{J} \quad uy\mathbf{I} + vx\mathbf{I} - xy\mathbf{J} \quad \dots}_{\text{second-order...}} \right)$$

$$\left(\underbrace{vy - \frac{y^2}{2}\mathbf{J}}_{\text{zero-order}} \quad \underbrace{uz\mathbf{I} + wx\mathbf{I} - xz\mathbf{J} \quad v\mathbf{I} + wy\mathbf{I} - yz\mathbf{J} \quad wz - \frac{z^2}{2}\mathbf{J}}_{\text{...second-order}} \right)$$

$$(\mathbf{G}_{000}, \mathbf{G}_{100}, \mathbf{G}_{010}, \mathbf{G}_{001}, \mathbf{G}_{200}, \mathbf{G}_{110}, \mathbf{G}_{020}, \mathbf{G}_{101}, \mathbf{G}_{011}, \mathbf{G}_{002}) =$$

$$\left(\underbrace{\mathbf{I}}_{\text{zero-order}} \quad \underbrace{x\mathbf{I} \quad y\mathbf{I} \quad z\mathbf{I}}_{\text{first-order}} \quad \underbrace{\frac{x^2}{2}\mathbf{I} \quad xy\mathbf{I} \quad \frac{y^2}{2}\mathbf{I} \quad xz\mathbf{I} \quad yz\mathbf{I} \quad \frac{z^2}{2}\mathbf{I}}_s \right) \text{second-order} \quad (50)$$

Again, the first-order approximation (sum of zero-order and first-order terms) leads to the affine-invariant approach of Günther and Theisel. For higher orders than shown here, use the general description in Eq. (48).

6 OTHER BASIS APPROXIMATIONS

6.1 Chebyshev Approximation

Aside from the Taylor approximation, we experimented with other function approximations, as discussed in Section 7.7 of the main paper. In order to adapt to spatial variations of \mathbf{F}_t , $\nabla \mathbf{F}_t$ and \mathbf{G} within the neighborhood U , we spatially discretize these derivatives by a multi-variate Chebyshev approximation in a neighborhood region U . Note that we have to normalize the entire domain to $[-1, 1]$, since the Chebyshev approximation only works well on that range. We get:

$$\mathbf{F}_t(\mathbf{x}, t) = \sum_{k=0}^{\infty} \sum_{j=0}^{\infty} \mathbf{c}_{k,j} T_k(x) \cdot T_j(y) \quad (51)$$

$$\nabla \mathbf{F}_t(\mathbf{x}, t) = \sum_{k=0}^{\infty} \sum_{j=0}^{\infty} \left[\mathbf{c}_{k,j} \frac{dT_k(x)}{dx} \cdot T_j(y) \quad \mathbf{c}_{k,j} T_k(x) \cdot \frac{dT_j(y)}{dy} \right] \quad (52)$$

$$\mathbf{G}(\mathbf{x}, t) = \sum_{k=0}^{\infty} \sum_{j=0}^{\infty} \mathbf{d}_{k,j} T_k(x) \cdot T_j(y) \quad (53)$$

with the Chebyshev polynomials and derivatives:

$$T_n(x) = \cos(n \cos^{-1} x), \quad \frac{dT_n(x)}{dx} = \frac{n}{1-x^2} \sin(n \cos^{-1} x) \quad (54)$$

Similar to the Taylor approximation, we call m the order of the terms, with $m = k + j$. Thus, an m -th order Chebyshev approximation sums up all terms up to m . Note that for $m = 0$ and $m = 1$, the Taylor approximation and the Chebyshev approximation are identical. As shown in Fig. 1a, we found that the Chebyshev approximation performed slightly worse than the Taylor approximation, and hence keep the Taylor approximation as default choice.

6.2 Fourier Approximation

Next, we apply a 2D Fourier approximation. For simplicity, we normalize the domain to $[-1, 1]$. We get:

$$\mathbf{F}_t(\mathbf{x}, t) = \sum_{k=0}^{\infty} \sum_{j=0}^{\infty} \mathbf{c}_{k,j}^{cc} C_k(x) \cdot C_j(y) + \mathbf{c}_{k,j}^{cs} C_k(x) \cdot S_j(y) \quad (55)$$

$$+ \sum_{k=0}^{\infty} \sum_{j=0}^{\infty} \mathbf{c}_{k,j}^{sc} S_k(x) \cdot C_j(y) + \mathbf{c}_{k,j}^{ss} S_k(x) \cdot S_j(y) \quad (56)$$

$$\mathbf{F}_{xt}(\mathbf{x}, t) = \pi \sum_{k=0}^{\infty} \sum_{j=0}^{\infty} \mathbf{c}_{k,j}^{sc} k C_k(x) \cdot C_j(y) + \mathbf{c}_{k,j}^{ss} k C_k(x) \cdot S_j(y) \quad (57)$$

$$- \pi \sum_{k=0}^{\infty} \sum_{j=0}^{\infty} \mathbf{c}_{k,j}^{cc} k S_k(x) \cdot C_j(y) + \mathbf{c}_{k,j}^{cs} k S_k(x) \cdot S_j(y) \quad (58)$$

$$\mathbf{F}_{yt}(\mathbf{x}, t) = \pi \sum_{k=0}^{\infty} \sum_{j=0}^{\infty} \mathbf{c}_{k,j}^{cs} C_k(x) \cdot j C_j(y) + \mathbf{c}_{k,j}^{ss} S_k(x) \cdot j C_j(y) \quad (59)$$

$$- \pi \sum_{k=0}^{\infty} \sum_{j=0}^{\infty} \mathbf{c}_{k,j}^{cc} C_k(x) \cdot j S_j(y) + \mathbf{c}_{k,j}^{sc} S_k(x) \cdot j S_j(y) \quad (60)$$

$$\mathbf{G}(\mathbf{x}, t) = \sum_{k=0}^{\infty} \sum_{j=0}^{\infty} \mathbf{d}_{k,j}^{cc} C_k(x) \cdot C_j(y) + \mathbf{d}_{k,j}^{cs} C_k(x) \cdot S_j(y) \quad (61)$$

$$+ \sum_{k=0}^{\infty} \sum_{j=0}^{\infty} \mathbf{d}_{k,j}^{sc} S_k(x) \cdot C_j(y) + \mathbf{d}_{k,j}^{ss} S_k(x) \cdot S_j(y) \quad (62)$$

with the sine and cosine basis functions:

$$C_n(x) = \cos(\pi n x), \quad S_n(x) = \sin(\pi n x) \quad (63)$$

Similar to the Taylor approximation, we call m the order of the terms, with $m = k + j$. Thus, an m -th order Fourier approximation sums up all terms up to m . We order the non-zero coefficients as:

$$\underbrace{\mathbf{c}_{0,0}^{cc}, \mathbf{d}_{0,0}^{cc}}_{m=1} \underbrace{\mathbf{c}_{1,0}^{cc}, \mathbf{d}_{1,0}^{cc}, \mathbf{c}_{0,1}^{cc}, \mathbf{d}_{0,1}^{cc}, \mathbf{c}_{0,1}^{cs}, \mathbf{d}_{0,1}^{cs}, \mathbf{c}_{1,0}^{sc}, \mathbf{d}_{1,0}^{sc}}_{m=2}} \quad (64)$$

$$\underbrace{\mathbf{c}_{2,0}^{cc}, \mathbf{d}_{2,0}^{cc}, \mathbf{c}_{1,1}^{cc}, \mathbf{d}_{1,1}^{cc}, \mathbf{c}_{0,2}^{cc}, \mathbf{d}_{0,2}^{cc}, \mathbf{c}_{1,1}^{cs}, \mathbf{d}_{1,1}^{cs}, \mathbf{c}_{0,2}^{cs}, \mathbf{d}_{0,2}^{cs}, \mathbf{c}_{2,0}^{sc}, \mathbf{d}_{2,0}^{sc}, \mathbf{c}_{1,1}^{sc}, \mathbf{d}_{1,1}^{sc}, \mathbf{c}_{1,1}^{ss}, \mathbf{d}_{1,1}^{ss}, \dots}_{m=3}} \quad (65)$$

For $m = 0$, the Fourier approximation is identical to the Taylor approximation. In the experiment in Fig. 1b, the Fourier approximation performed worse than the Taylor approximation. Further, it has more unknowns due to the sine/cosine basis pairs and is therefore slower. Thus, we kept the Taylor approximation as the default option.

7 ANALYTIC VECTOR FIELDS

In the following section, we further define the constructed unsteady vector fields used in Section 7 of the main paper.

7.1 Modified Double Gyre

Inspired from Shadden's Double Gyre [2], we now construct a MODIFIED DOUBLE GYRE for our analytical ground truth topology. Shadden

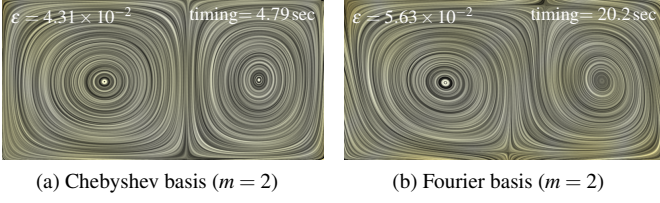


Fig. 1: Comparison of the second-order approximations with the Chebyshev (1a) and Fourier basis (1a).

defined a steady vector field as co-gradient of a stream function:

$$\mathbf{v}^*(\mathbf{x}^*, t) = \begin{pmatrix} -\pi A \sin(\pi x^*) \cos(\pi y^*) \\ \pi A \cos(\pi x^*) \sin(\pi y^*) \end{pmatrix} \quad (66)$$

and introduced a deformation $f(x, t)$ to move the x -coordinate in the stream function formulation, with $f(x, t) = a(t)x^2 + b(t)x$, $a(t) = \varepsilon \sin(\omega t)$, and $b(t) = 1 - 2\varepsilon \sin(\omega t)$. By deforming the stream function, the resulting time-dependent co-gradient vector field is divergence-free. However, this construction approach cannot control the location of features, such as vortex corelines and bifurcation lines. Instead, we define a displacement field $\mathbf{F}(\mathbf{x}, t) = (f(x, t) - x, 0)^T$ and apply Eq. (10) to compute our unsteady vector field $\mathbf{v}(\mathbf{x}, t)$:

$$\mathbf{v}(\mathbf{x}, t) = \begin{pmatrix} \frac{-\pi A \sin(\pi f(x, t)) \cos(\pi y) + x(2-x)\varepsilon \omega \cos(\omega t)}{2a(t)(x-1)+1} \\ \pi A \cos(\pi f(x, t)) \sin(\pi y) \end{pmatrix} \quad (67)$$

In the main paper, we have shown that critical lines in the optimal frame $\mathbf{w}(\mathbf{x}, t)$ are pathlines of $\mathbf{v}(\mathbf{x}, t)$. In the domain $[0, 2] \times [-1, 1]$, vortex corelines pass through $(x, y, t) = (1 \pm 0.5, \pm 0.5, 0)$, and a bifurcation line passes through $(x, y, t) = (1, 0, 0)$. In our experiments, we set $A = 0.1$, $\varepsilon = 0.25$ and $\omega = 2\pi/10$.

7.2 Deforming Centers

The first example is based on the four centers flow [1], where we construct an unsteady flow by transforming the co-gradient of the stream function $s^*(\mathbf{x}^*, t) = 3xy \cdot e^{-x^2 - y^2}$ with the spatially-varying displacement transformation $\mathbf{F}(\mathbf{x}, t)$:

$$\mathbf{F}(\mathbf{x}, t) = \begin{pmatrix} \cos(2t) - 1 & -\sin(2t) \\ \sin(2t) & \cos(2t) - 1 \end{pmatrix} \cdot \begin{pmatrix} 0 \\ \frac{1}{10}x^2t + \frac{1}{5}xt \end{pmatrix} \quad (68)$$

which not only rotates the domain but also has structures moving at different speed based on their location. Results using this flow are shown in Fig. 8 of the main paper.

7.3 Sink-Source-Saddle Flow

To study the separatrices in a compressible vector field containing sinks, sources and saddles, we construct a vector field where the separatrices are curved lines. For this, we use the steady vector field:

$$\mathbf{v}^*(\mathbf{x}^*, t) = \frac{1}{128} \begin{pmatrix} -(y^3 + 8x - 8)(y^3 + 16x + 16) \\ -(x^3 + 8y - 8)(x^3 + 16y + 16) \end{pmatrix} \quad (69)$$

and transform it with the following spiraling transformation:

$$\mathbf{F}(\mathbf{x}, t) = \begin{pmatrix} \cos\left(\frac{tx^2 + ty^2}{10}\right) - 1 & -\sin\left(\frac{tx^2 + ty^2}{10}\right) \\ \sin\left(\frac{tx^2 + ty^2}{10}\right) & \cos\left(\frac{tx^2 + ty^2}{10}\right) - 1 \end{pmatrix} \begin{pmatrix} x \\ y \end{pmatrix} \quad (70)$$

Results using this flow are shown in Fig. 9 of the main paper.

7.4 Vortex with Changing Magnitude

We studied an analytic vortex based on Vatasias [3] experimentally-obtained velocity profile. In this example, the vortex is not moving, but

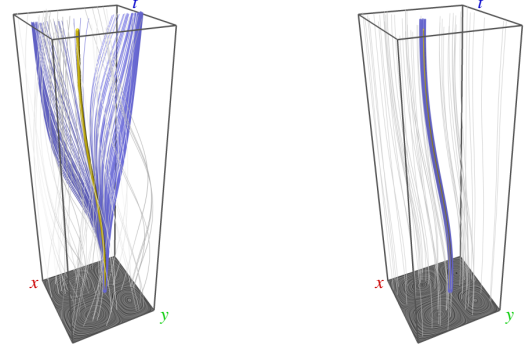


Fig. 2: Bifurcation lines (ground truth in yellow) are tangential to both the original flow $\mathbf{v}(\mathbf{x}, t)$ and the ambient motion field $\mathbf{f}(\mathbf{x}, t)$. Tracking bifurcation lines is much more stable in $\mathbf{f}(\mathbf{x}, t)$, since pathlines in $\mathbf{v}(\mathbf{x}, t)$ deviate away from saddles along the repelling eigenvector direction. Blue pathlines are seeded close to the bifurcation line at the bottom of the space-time domain. Further gray pathlines are given as context.

its tangential velocity changes over time. The flow $\mathbf{v}(\mathbf{x}, t)$ is considered in the domain $[-2, 2]^2 \times [0, 10]$:

$$\mathbf{v}(\mathbf{x}, t) = \frac{t}{2} \begin{pmatrix} -y \\ x \end{pmatrix} \frac{v_0(\sqrt{x^2 + y^2})}{\sqrt{x^2 + y^2}}, \quad v_0(r) = \frac{r}{2\pi r_c^2 \left(\left(\frac{r}{r_c} \right)^{2n} + 1 \right)^{\frac{1}{n}}}$$

with shape coefficient $n = 2$ and core radius $r_c = 1$. Results using this flow are shown in Fig. 10 of the main paper.

8 MORE RESULTS

In this section, we report further experiments and results using our reference frame optimization and vector field topology extraction.

8.1 Bifurcation Line Tracing

In the main paper, we found that critical paths can be tracked in space-time as pathlines in the input unsteady flow $\mathbf{v}(\mathbf{x}, t)$ or in the ambient motion $\mathbf{f}(\mathbf{x}, t)$. The integration in $\mathbf{v}(\mathbf{x}, t)$ can be extremely unstable, for instance, when tracing along a bifurcation line, since a tiny numerical error would lead to an exponential push off the bifurcation line. The field $\mathbf{f}(\mathbf{x}, t)$, on the other hand, follows the feature on and in the vicinity of the critical point, see for instance in Fig. 2. Thus, using our ambient motion field, the integration of bifurcation lines becomes more stable. Stable feature flow fields [4] could further reduce integration errors.

8.2 Dependence on Temporal Resolution

In the following, we study how the temporal resolution of the data set affects the reference frame optimization. Fig. 3 shows the near-steady vector fields $\mathbf{w}(\mathbf{x}, t)$ of our third-order displacement optimization for varying temporal resolutions in the CYLINDER 2D flow. Each frame lists the temporal distance between consecutive time steps. The difference between $\Delta t = 0.01$ (used in the paper) and $\Delta t = 0.04$ is barely visible. For larger differences, artifacts become significant. A good temporal resolution is as important as a high spatial resolution to track features in space-time.

8.3 Separatrices and FTLE Ridges

The main paper showed the PIPED CYLINDER data set, a flow that goes around two corners and passes two cylinder obstacles. Fig. 4 shows a time slice of this flow. In the top row, we see our flow in the optimal frame $\mathbf{w}(\mathbf{x}, t)$, containing vortex centers and saddles. We can see that ridges in the forward and backward FTLE align with the separatrices in our optimal frame $\mathbf{w}(\mathbf{x}, t)$. In the bottom row, we see the ambient motion field $\mathbf{f}(\mathbf{x}, t)$, showing how the vortices are transported through the gap between the two corners. Arrows indicate the magnitude of $\mathbf{f}(\mathbf{x}, t)$.

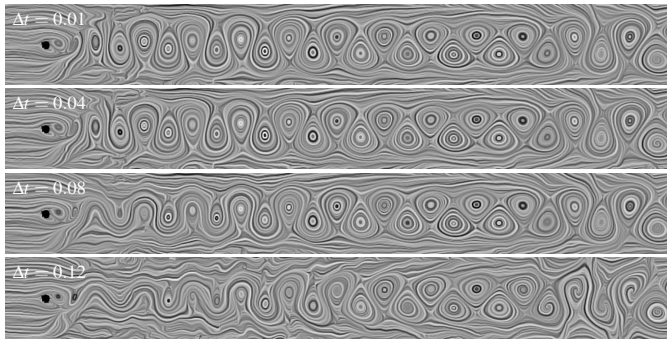


Fig. 3: Comparison of the reference frame extraction for varying temporal resolutions. For each image the temporal distance Δt between two consecutive time steps is listed. The larger the distance, the more artifacts occur. In the main paper, we used $\Delta t = 0.01$.

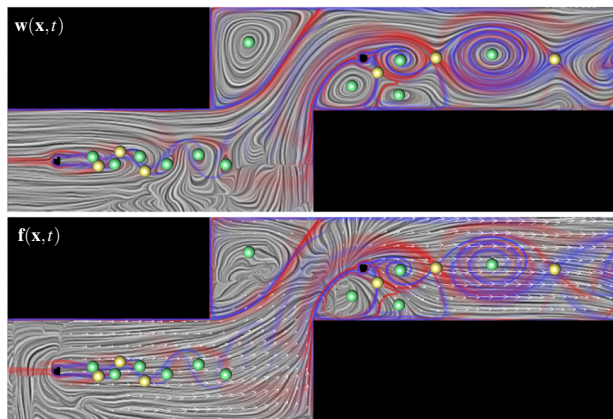


Fig. 4: Time slice in the PIPED CYLINDER flow showing vortex centers (green), saddles (yellow), forward FTLE (red) and backward FTLE (blue). The top row shows the flow in the optimal frame $w(x, t)$ and the bottom row shows the ambient motion field $f(x, t)$ with arrows to indicate the magnitude of $f(x, t)$.

8.4 Tracking of Feature Curves with Ambient Flow

In the main paper, we traced the paths of 3D vortex corelines and bifurcation lines in the ambient motion field $f(x, t)$ of the SQUARE CYLINDER flow. In Fig. 5, we show a second set of feature curves that have been extracted at a later time step. We can see that the feature curves lie very close to the path surface of the ambient motion field. Note, however, that we extract the feature curves per time slice without enforcing temporal smoothness. We can therefore expect some jittering that we discussed in the limitations section.

8.5 Topology in a Turbulent Flow

Fig. 6 shows results obtained with our second-order displacement optimization in the ROTATING MIXER flow. Topological elements were extracted in w (left) and the ambient motion of the vortex corelines is visualized via short pathsurfaces in f (right). In such turbulent flows, a large number of topological structures occur, including the vortex corelines and the critical points. The amount of visual clutter limits the applicability of topology-based methods in turbulent flows, which is a general limitation of topology-based approaches.

REFERENCES

- [1] T. Günther, M. Schulze, and H. Theisel. Rotation invariant vortices for flow visualization. *IEEE Transactions on Visualization and Computer Graphics (Proc. IEEE SciVis 2015)*, 22(1):817–826, 2016.
- [2] S. C. Shadden, F. Lekien, and J. E. Marsden. Definition and properties of Lagrangian coherent structures from finite-time Lyapunov exponents in two-dimensional aperiodic flows. *Physica D: Nonlinear Phenomena*, 212(3-4):271–304, 2005.

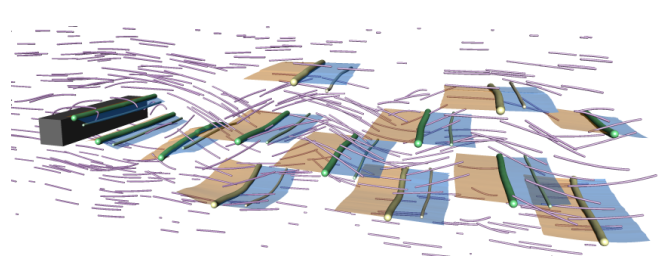


Fig. 5: The motion of the features curves (orange and blue) is extracted as pathsurfaces in $f(x, t)$. A second set of feature curves with smaller radius shows the location of features at a later time. As context, we show purple pathlines in $v(x, t)$ (right).

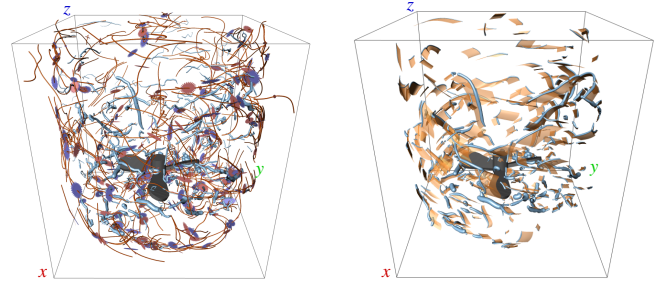


Fig. 6: Example in the ROTATING MIXER flow showing vortex corelines, critical points and separatrices (left) and the ambient motion of the corelines (right). In turbulent flows, standard topology is not a suitable method due to the large number of features.

- [3] G. H. Vatistas, V. Kozel, and W. Mih. A simpler model for concentrated vortices. *Experiments in Fluids*, 11(1):73–76, 1991.
- [4] T. Weinkauff, H. Theisel, A. V. Gelder, and A. Pang. Stable feature flow fields. *IEEE Transactions on Visualization and Computer Graphics*, 17(6):770–780, 2011.